THE PHYSICAL BASIS OF THE EXPLOSION SOURCE AND GENERATION OF REGIONAL SEISMIC PHASES

Jeffry L. Stevens, G. Eli Baker, Heming Xu, and Theron J. Bennett

Science Applications International Corporation

Sponsored by Air Force Research Laboratory

Contract No. FA8718-04-C-0025

ABSTRACT

The objective of this project is to determine the source physics and corresponding generation and evolution of local and regional seismic waves from nuclear explosions. In particular, we want to explain the source of the explosion-generated Lg phase. In a previous project we identified the following contributing sources to Lg: surface reflected pS that is trapped in the crust, S*, scattered Rg, and shear waves directly generated by non-spherical source elements. Our goal now is to quantify the contribution of each to Lg under different source conditions. To this end we have performed work in several complementary areas.

The Russian Institute for the Dynamics of the Geospheres (IDG) has provided yield and depth information for 11 Degelen and 4 Balapan explosions. They have digitized records on their near regional stations (50-100 km distance) for all four Balapan explosions and one of the Degelen explosions. They have also provided near source peak particle velocities, rise times, and positive pulse duration measurements from ten Degelen nuclear explosions. These explosions were all conducted in high velocity media (>5 km/sec P velocity) and therefore place important constraints on the Lg generation problem. The Balapan near regional data provides a contrast with existing near regional Degelen explosion data. As the source media are similar while the near source topographies differ, these data may be useful in distinguishing the role of topography in near source scattering. The new near field measurements and near regional records provide an opportunity to track differences between Balapan and Degelen regional records back to their source.

In a closely related analysis, to assess whether the amount of shear waves generated is affected by source depth and/or scaled depth, we examine the regional phase amplitudes of 13 Degelen explosions with known yields and source depths. The events range from 20% to 50% underburied. Preliminary analysis shows similar $\log_{10}$ amplitude vs. $\log_{10}$ yield curves for the initial Pn, the entire P wavetrain, Sn, Lg, and Lg coda. The slope of those curves varies with frequency, ranging from approximately 0.84 at 0.6 Hz to 0.65 at 6 Hz. We perform nonlinear source calculations to complement these observations, aimed at determining constraints on the relative size of CLVD and explosion sources.

We have also examined recordings of historical co-located decoupled and tamped explosions at Azgir in the former Soviet Union, utilizing all 3 components of data and focusing on differences in shear wave generation between the explosions. The relative S to P wave amplitude appears similar at low frequencies, but is much greater above 8 Hz for the tamped explosion, although interpretation is complicated by the frequency dependence of the decoupling. The tamped explosion also has clear Sn at regional distances. No similar records were available for the decoupled explosion. The tamped explosion, at 64 Kt and 987 m depth in salt, was 2 times overburied. Even if it were tamped, the 10 Kt decoupled explosion would have been nearly 4 times overburied. Wavenumber synthetic seismograms show that generation of the observed shear waves by a spherical explosion source is implausible, even in very complex source structure. We plan to perform nonlinear source calculations to assess the possibility of non-spherical source terms, at the surface and at an interface between the salt and overlying sediments.

Finally, we model scattering of Rg into Lg for known source areas and compare resulting synthetics with regional data. We use an approximation based on modal scattering of fundamental mode Rg into higher mode Lg, using as constraints estimates of Rg decay rates from Degelen and deep seismic sounding explosions. The goal of this analysis is to quantify the contribution of Rg to Lg in different areas with different earth structures.

OBJECTIVE

The objective of this project is to determine the source physics and corresponding generation and evolution of local and regional seismic waves from nuclear explosions. This is a joint project between Science Applications International Corporation (SAIC) and IDG in Moscow, Russia.

RESEARCH ACCOMPLISHED

Introduction

We are in the first year of a new project to determine the source physics and corresponding generation and evolution of local and regional seismic waves from nuclear explosions. This is a joint project between SAIC and IDG in Moscow, Russia. The project continues work initiated under two previous projects: 1) a joint project between SAIC and IDG to digitize and analyze a large data set of near field (35-900 meters) and near regional (10-100 km) waveforms from Degelen mountain explosions (Stevens et al., 2003; and 2) a project to determine the source of explosion-generated Lg using numerical modeling and data analysis (Stevens et al., 2004b).

In the previous joint project, IDG provided an exceptional historical data set of 192 near field and near regional records of 23 Degelen mountain nuclear explosions. In the current project, IDG is providing near field measurements from 26 Degelen Mountain explosions, and near regional waveforms from 10 Balapan explosions, together with explosion yields and depths where available for each event. We are using the near regional data from Degelen and Balapan to assess the evolution of different seismic phases over this distance range, the variability of seismic phases, and the differences in source function and regional waveforms due to differing media at the two test sites. We are also using IDG data from the Degelen test site to investigate the effect of explosions located close enough together that the first explosion could have affected the rock properties near the second explosion. Previous studies of Lg generation have been dominated by studies of Nevada Test Site (NTS) explosions because of the availability of data and good control on source media and explosion yields. The data and information provided by IDG are particularly important because they relate to nuclear explosions in high velocity source media, and in a region of interest.

Lg consists of shear waves trapped in the crust and observed at regional distances. It is important to treaty monitoring because 1) Lg amplitudes have been found to correlate with explosion yield better than other phases; and 2) Lg spectral characteristics and Lg/P spectral ratios are important regional discriminants. However, without a clear physical understanding of the source of Lg, use of these procedures in uncalibrated areas is questionable and errors are likely.

In the previous Lg generation project, we made considerable progress in understanding explosion-generated shear waves by quantifying and numerically reproducing features of observations of shear waves generated under different source conditions. In the current project, we are trying to quantify the results and determine the implications for the transportability of explo`sion yield estimation and discrimination. We are using the large data set of local and regional signals from nuclear explosions collected under the previous contract, combined with the new Russian data, to improve our understanding of the explosion source and to assess the contributions of different mechanisms for generation of Lg under different source conditions.

A simple point explosion generates no shear waves, so the Lg phase is generated entirely by non-spherical components of the source and conversions through reflections and scattering. The most important contributors to the Lg phase are:

- P->S conversion at the free surface and other near source interfaces.
- S waves generated directly by a realistic distributed explosion source including nonlinear effects due to the free surface and gravity.
- Rg scattering to Lg.

Each of these sources is sensitive, in different ways, to source region structure, near regional path characteristics, source depth, scaled depth, and yield. For example, Lg generated by P->S conversion depends on the source region velocity relative to the mantle velocity; S waves generated by the source are sensitive to scaled depth; Lg generated by Rg scattering depends on source depth and the near regional scattering rate. These effects can be quantitatively modeled and constrained by known information about the source and source region.

In addition to source and near source effects, Lg is affected by scattering and conversion along the travel path. The most important effects are:

- S->S scattering that changes the orientation and direction of the near source P-to-S converted waves, affecting the extent to which they are trapped in the crust.
- Randomization of the components of Lg.

Both effects tend to homogenize the observations of Lg. For example, S waves generated by P->S conversion at the free surface in a high velocity structure leak to the mantle, but S->S scattering reduces this effect by changing the ray direction and allowing more S to be trapped. Randomization of Lg orientation reduces differences between the components. In addition to the effects listed here, a variety of other scattering modes including P->S conversion along the path and Lg scattering also contribute to Lg and Lg coda.

Our goal in this project is to quantify the contribution of each of the major source mechanisms for Lg, determine the amount of variation in each with changes in source region structure, near regional path characteristics, source depth, scaled depth, and yield, compare predictions with data, assess the effects of path contributions to Lg, and evaluate the implications of the results for discrimination and explosion yield estimation.

New data from IDG

IDG is providing data and related information from the Soviet nuclear test program. To date, they have delivered the data listed in Table 1, including near field tabular data of particle velocity and rise time from 10 Degelen explosions, near regional seismic records from one Degelen and four Balapan explosions, and the explosion yields and depths for these events. Figure 1 shows an example of the data.

Table 1. Data collected by IDG

Date	Yield (kt)	Depth (m)	Site	Rock Type
1961/10/11	1.16	141	D	G
1962/02/02	16.9	265	D	G
1964/06/06	1.05	75	D	G
1964/11/16	23	203	D	QP
1965/02/04	17	262	D	G
1965/02/04	1.0	126	D	G
1965/09/17	10	148	D	QP
1966/02/13	109-125	343	D	QP
1967/12/08	12.5	166	D	QP
1968/09/29	75	358	D	QP
1985/07/20	76	466	D	
1988/04/22	2	---	B	
1988/09/14	140	651	B	
1989/01/22	108	580	B	
1989/02/12	74	572	B	

D stands for Degelen
B stands for Balapan
G stands for Granite
QP stands for Quartz Porphyry

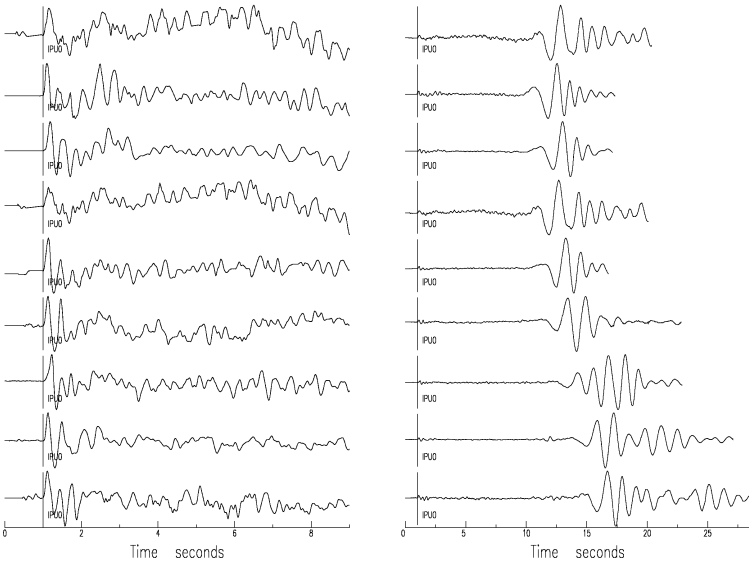

Figure 1. Vertical component records, from 58 to 88 km distance, of the 1989/01/22 Balapan explosion. Rg dominates (right), so initial segments of the records cut off before the Rg arrival are also plotted (left). Unlike most of the Degelen explosions, there is no clear S-wave phase between the P and Rg.

Numerical modeling of the explosion source

One of the major contributors to generation of shear waves by explosions is the effect of the free surface and gravity. This causes a very substantial vertical asymmetry in the source. We are investigating the effect of depth, scaled depth, and material properties on generation of shear waves from a realistic explosion source. Figure 2 shows regions of nonlinear deformation and cracking from two nonlinear source calculations, and Figure 3 shows waveforms calculated for these calculations. The calculations were performed in a structure with material properties

appropriate for the Degelen test site at the same depth (300 meters) but for different yields (31 kt and 112 kt) and therefore different scaled depths. Normal containment depth is approximately 122 $W^{1/3}$ meters where W is yield in kilotons, so the explosions are both underburied at 78% and 51% of normal scaled depth, respectively.

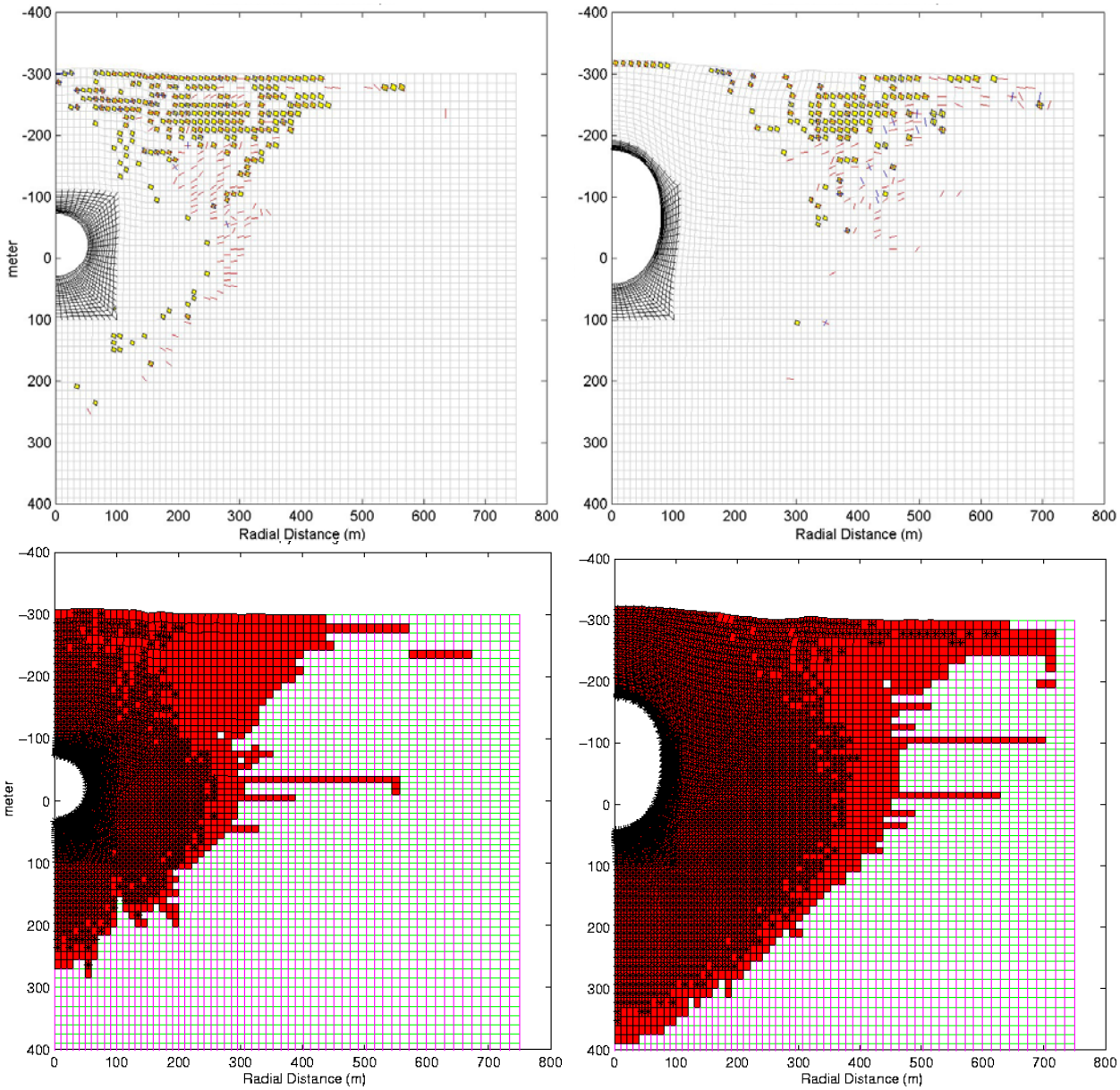

Figure 2. Near source permanent deformation due to cracking (upper) and yielding (lower) for explosions in a granite halfspace, at 78% (left) and 51% (right) of source depth. In the cracking images, yellow squares indicate hoop cracks, and red and blue lines indicate radial and in-plane tangential cracking respectively. Grid lines in both plots were initially straight. Their positions shown above represent the permanent displacement after the explosions.

Note the strong distortion of the cavity by the larger event. Both events generate strong S phases, and the Lg to P ratios are similar. This suggests that S generation is both strong and relatively independent of scaled depth for normal to underburied explosions. However, as we showed previously (Stevens et al., 2004b), generation of S does decrease for overburied explosions. All of the Degelen explosions that we analyzed are underburied, while the Balapan explosions that we will be analyzing are more commonly normally or slightly overburied.

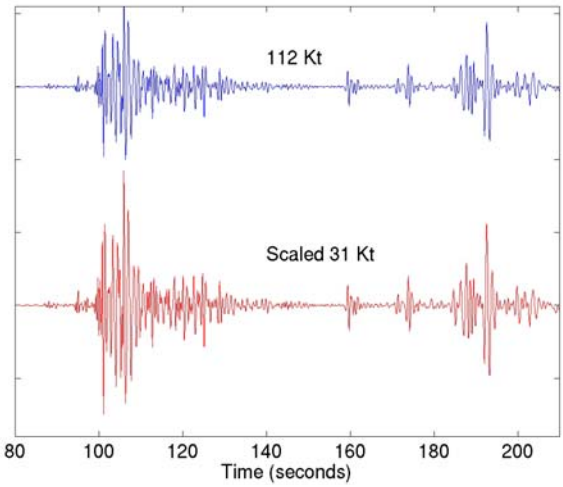

Figure 3. Seismograms calculated from the 112kt (top) and 31 kt (bottom) calculations at a distance of 650 km. The 31 kt seismogram has been scaled by a factor of 112/31.

Amplitude vs. yield, depth, and extent of underburial for 14 Degelen Mt. explosions recorded at BRVK

We examined 41 vertical component seismograms recorded at BRVK (650 km) of 14 Degelen nuclear explosions for which there exist reported yields. Thirteen of the events also have a reported depth. The multiplicity of recordings on 8 different types of instruments provides redundancy and so improves confidence in correlations. We measured amplitudes of Pn (first 5 seconds), the entire P wavetrain (first break to 5.4 km/s group velocity), Sn (first 10 seconds after the picked arrival time), Lg (3.6 to 3.0 km/s), and Lg coda (3.0 to 2.5 km/s). Amplitudes were converted to microns using reported gains and response curves at the frequency of observation.

There are consistent offsets between the amplitudes recorded on different instruments, reflecting systematic errors in reported gains of some, or all, instruments. The slope of the $\log_{10}$ amplitude vs. $\log_{10}$ yield curves for each instrument type are similar for each phase and frequency, so we use the amplitudes of all the phases and a constant slope of the $\log_{10}$ amplitude vs. $\log_{10}$ yield curve for each frequency to determine offsets of each instrument. These offsets were used to correct $\log_{10}$ amplitude measurements from all other instruments to that of the KS instrument, which was the most common. The corrections are approximately 3% to 5% of the individual $\log_{10}$ phase amplitudes, and should aid in detecting trends in amplitude with yield, source depth, or source depth relative to scaled depth.

Log_{10} amplitude vs. $\log_{10}$ yield curves were calculated using all 41 records, and again for just the 26 records made with the 4 instruments (KS, SBU-V, SKM, and SVKSMt) that had the most recordings and the most consistent amplitude offsets relative to other records. Figure 1 shows the slopes of those curves for a range of frequencies. Many of the explosions had multiple recordings, so at each frequency, a single amplitude was determined for each phase based on the median of the amplitudes after corrections to the KS instrument. That provided up to 14 amplitudes for each phase for comparison with yield. These values were bootstrapped 1000 times. The colored squares in each plot represent the median slope of all the bootstrapped outcomes. The confidence bounds represent the 25^{th} and 75^{th} percentiles, and are generally smaller for the P-wave measurements than for the S wave phases. The ratio of Lg signal to pre-Lg noise amplitudes dropped below 1.5 above 2.4 Hz. Figure 2 shows examples of the data on which the above analysis is based, the $\log_{10}$ amplitudes at 0.6 and 2.4 Hz of the each phase vs. $\log_{10}$ yield.

The slope of the $\log_{10}$ amplitude vs. $\log_{10}$ yield curve as a function of frequency, based on all phases and all recordings, with weighting for data quality, is $s = 0.855 - 0.034*f$, where s is slope and f is frequency. This provides a slope of 0.84 at 0.6 Hz, and a slope of 0.65 at 6 Hz. Various weightings of the data produce similar relationships.

Lg coda is larger than the P phases at low frequency, but much smaller at high frequency. This may mirror a change in its composition. At low frequency it stands out in the seismogram and is likely composed of similar waves to Lg that could be modeled as higher-mode surface waves. At higher frequencies, its amplitude is monotonically decreasing with time and is more like typical coda, commonly considered to be composed of multiply scattered

shear waves. The entire P wavetrain is made up of Pn and Pg. Their relative contributions vary from low frequency, where both appear significant, to high frequency where Pn appears to dominate.

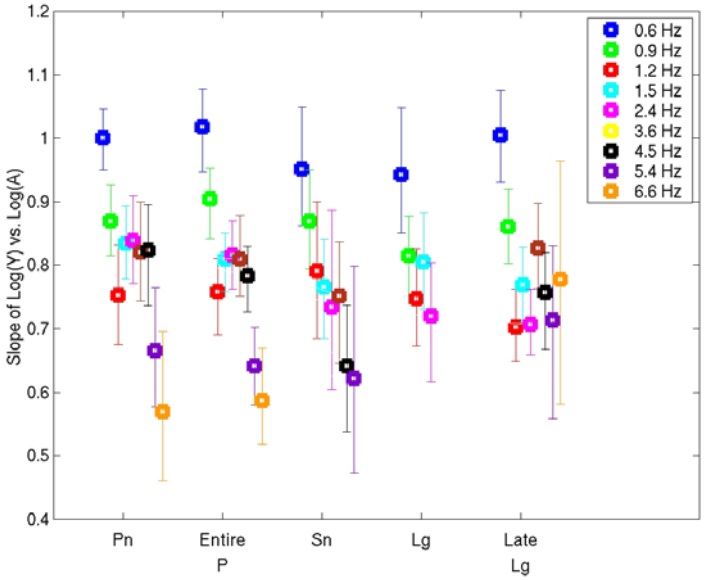

Figure 4. Slopes of the $\log_{10}$ amplitude vs. $\log_{10}$ yield curves for each phase and for a range of frequencies, using all 41 records available.

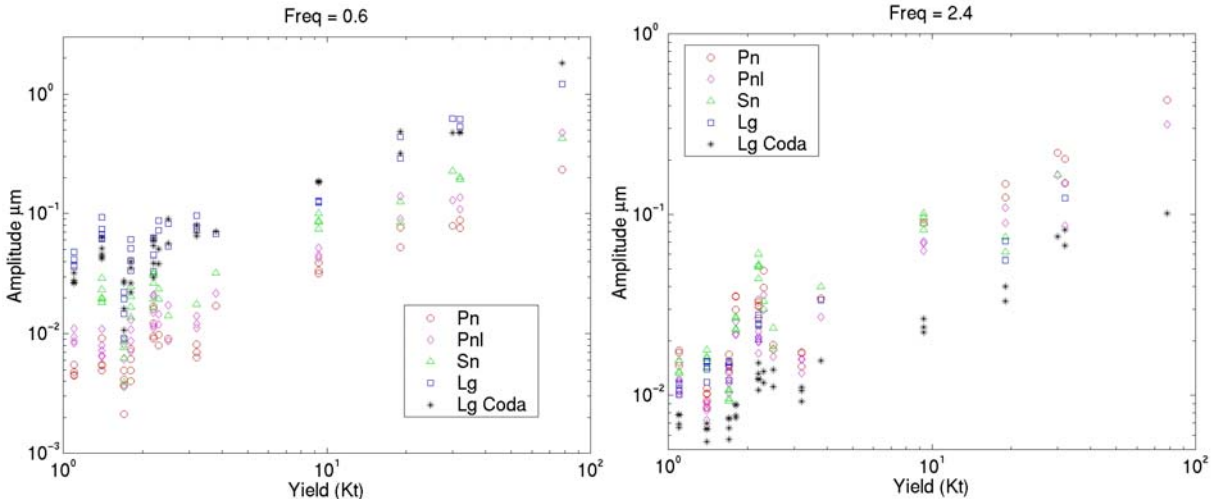

Figure 5. amplitude vs. yield curves for each phase at 0.6 Hz (left) and 2.4 Hz (right). The slopes are all similar, but the shear wave curves are higher at 0.6 Hz and the P wave curves are higher at 2.4 Hz.

For each phase, we determined an amplitude-yield relation using the same predicted slope of the $\log_{10}$ amplitude vs. $\log_{10}$ yield curve, s= 0.855 - 0.034*f, but with a different intercept determined for each phase. Residual amplitudes for each phase were then compared with depth, the extent to which the event was underburied, and yield. No statistically significant dependence is apparent between amplitudes of any of the phases and depth, yield, or extent of underburial. No strong dependence is apparent between ratios of the different phases and the parameters, although Lg/Lg Coda ratios at 1.1 Hz, and Sn/Pn ratios at 2.4 and 3.7 Hz appear to decrease slightly with depth and yield. More data are necessary to determine whether this observation can be substantiated.

Table 2 shows the median of the yield residuals for each phase with 2 smad error bounds on the median, for a range of frequencies. This is based on a common set of recordings for each phase. We use only those records with signal-to-noise ratio greater than 1.5 for all phases for the first 4 frequencies, and for Pn, the entire P wavetrain, Sn, and Lg coda at the higher frequencies (where Lg drops below the pre-Lg noise level). Pre-event noise is used to assess S/N

for Pn, Pnl, and Lg Coda. Pre-Sn and pre-Lg windows are used to assess S/N for those two phases. The yield errors are smallest for the entire P wavetrain, except for the 3 highest passbands, where the coda based estimate is more accurate. Below 1 Hz, Lg and Sn yield estimates have at least twice the error of the P wavetrain. They are closer in accuracy at 1.2 and 1.5 Hz, and the Lg error is comparable at 2.4 Hz.

Table 2. Median Log_{10} yield errors +/- 2 SMAD.

Hz	npts	Pn	Pnl	Sn	Lg	Lg Coda
[1]0.6	32	0.10±0.05	0.07±0.03	0.18±0.10	0.18±0.08	0.12±0.05
0.9	18	0.11±0.10	0.05±0.04	0.13±0.05	0.10±0.07	0.07±0.04
1.2	27	0.19±0.09	0.08±0.05	0.13±0.07	0.11±0.06	0.12±0.05
1.5	24	0.11±0.08	0.07±0.04	0.12±0.07	0.11±0.06	0.12±0.05
2.4	22	0.15±0.09	0.09±0.06	0.22±0.14	0.09±0.05	0.11±0.07
3.6	34	0.08±0.05	0.06±0.03	0.12±05	*	0.10±0.05
4.5	34	0.10±0.05	0.09±0.04	0.16±0.08	*	0.08±0.04
5.4	29	0.13±0.08	0.12±0.07	0.14±0.08	*	0.06±0.03
[1]6.6	23	0.12±0.08	0.12±0.08	0.07±0.06	*	0.09±0.07

[1] 0.6 Hz is at or below the low frequency corner of most of the instruments, and 6.6 Hz is at the upper end of most of the known response curves, so the calibrations applied to these measurements may be less accurate than those at the intermediate frequencies.

* insufficient signal at common instruments over a large yield range

Rg-to-Lg scattering

We are attempting to model Rg to Lg scattering using a mode conversion model constrained by observations in different regions. Observations provide the Rg decay rate, a critical parameter in the modeling. Modeling results will be compared with Lg waveforms. We anticipate that widely varying decay rates in Eurasia vs. the western U.S. will lead to different Rg-to-Lg predictions. For example, Rg is observed at 650 km from the larger Degelen explosions (e.g., Figure 6), while it is difficult to distinguish Rg at local distances to NTS explosions. The near field Degelen and Balapan records, and Deep Seismic Sounding data will provide Rg decay rate values in Eurasia. A previous upper bound calculation (Stevens et al., 2004b) based on instantaneous scattering of all Rg into higher modes in an NTS structure, found that scattered Rg most strongly affects late Lg (later than 3 km/s) at frequencies below 1 Hz.

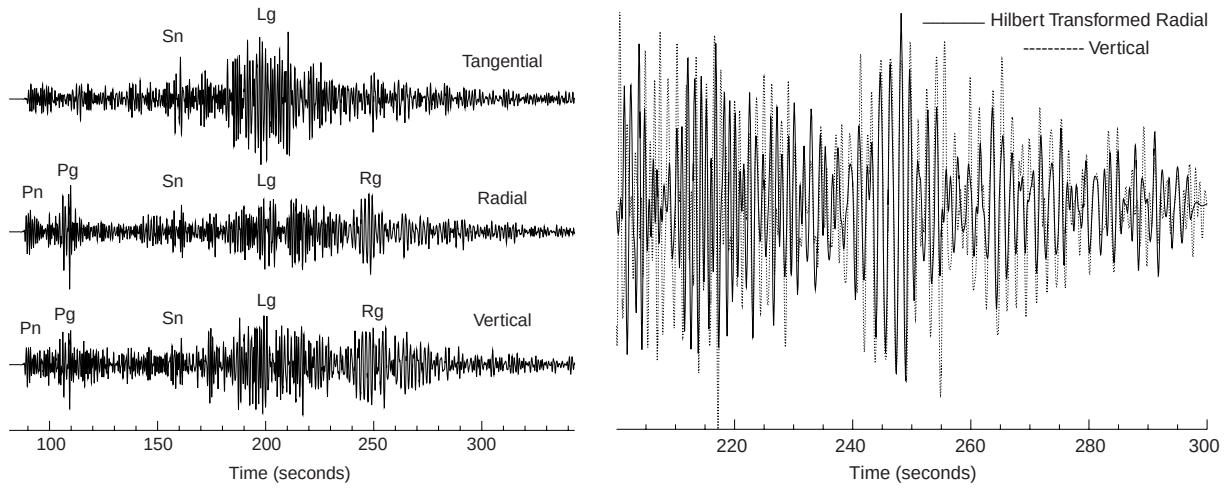

Figure 6. 3-component records (left) of a 90 Kt Degelen explosion on 4/25/1971, recorded at 651 km, at 0.5 Hz to 1 Hz. The vertical and Hilbert transformed radial seismograms (right) from 3.26 to 2.17 km/sec group velocities overlay from 240 seconds (~2.7 km/sec) onward, confirming identification of Rg in that window.

We model Rg to Lg scattering under the assumption that Lg is generated by a distribution of surface scatterers and that all energy scattered from Rg is converted to Lg. We make the following assumptions:

1) The explosion may be a complex source, but has a known source function and is located at the origin.
2) Scattering occurs on the earth's surface and can be modeled as generated by a distribution of vertical point sources.
3) No energy is lost in scattering.

All scattering is from Rg to higher modes. We neglect secondary scattering and scattering to leaky phases. We therefore consider that the scattered Rg consists of waves from a cylindrical distribution of point forces at the location of the propagating Rg phase (Figure 7), and that the scattered Rg goes into higher modes. These are optimistic assumptions and should be regarded as providing an upper bound on Lg generated by Rg scattering.

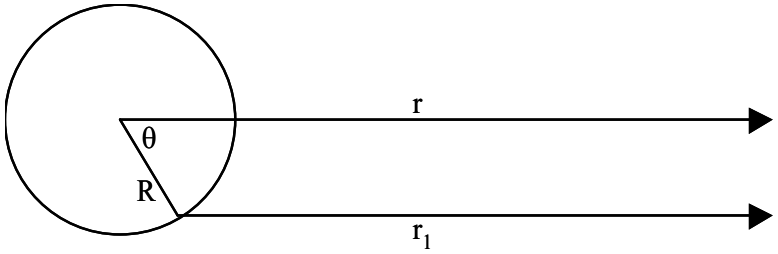

Figure 7. Rg propagates from the origin to radius R where it is scattered to Lg.

The vertical displacement from the initial Rg wave u_z^0 has the form

$$u_z^0(\omega,z,r) = A_0(\omega)G_s(r)\exp(-ik_0r-\gamma_0r)E_2(k_0,z)/\sqrt{r}\ , \tag{1}$$

where k_0 is the wave number ω/c, ω is the angular frequency, z is the depth, E_2 is the Rayleigh wave vertical displacement eigenfunction which is normalized to 1 at the free surface z=0, and A_0 is amplitude spectrum which depends on characteristics of the source and source region earth structure. γ_0 is the intrinsic attenuation function of Rg. G_s is a function that represents the attenuation of Rg due to scattering. The radial displacement has a similar form with E_2 replaced by the radial eigenfunction E_1. The kinetic energy T in the mode at location r is given by

$$T_0 = \tfrac{1}{2}\omega^2\int_0^\infty \rho(|u_z|^2+|u_r|^2)dz = \pi\omega^2G_s^2(r)\exp(-2\gamma_0r)|A_0(\omega)|^2\ I_1^0\ , \tag{2}$$

where I_1^0 is the energy integral on the left with the superscript indicating the fundamental mode. I_1 is the notation used by Takeuchi and Saito (1972) for this integral.

If part of u_z^0 is converted to a sum of higher modes u_z^1 at point R, we have

$$u_z^{\ 1} = \iint dRd\theta\sum_{i=1}^{N} S(\omega,R)\alpha_i(\omega)\exp(-ik_0R-ik_ir_1-\gamma_ir_1)E_2^i(k_i,z)/\sqrt{r_1}\ , \tag{3}$$

where α_i are modal coefficients corresponding to a vertical point force and S is the excitation function related to the energy transfer. Assuming azimuth independence of scatterers and neglecting small differences in attenuation and geometric spreading between r and r_1, we get:

$$u_z^{\ 1} = \frac{2\pi}{\sqrt{r}}\sum_{i=1}^{N}\alpha_i(\omega)\exp(-\gamma_ir-ik_ir)E_2^i(k_i,z)\int_0^\infty dRJ_0(k_iR)\exp(-ik_0R)S(\omega,R) \tag{6}$$

where J_0 is the Bessel function. The converted wave has a total energy of

$$T^1 = 4\omega^2\pi^3\sum_{i=1}^{N}\left|\alpha_i(\omega)^2\right|\left|I_1^i\exp(-2\gamma_ir)\right|\left|\int_0^\infty dRJ_0(k_iR)\exp(-ik_0R)S(\omega,R)\right|^2 \tag{7}$$

The Rg energy loss rate due to scattering at R is

$$\frac{dT_0}{dR} = 2\pi\omega^2|A_0(\omega)|^2\ I_1^0G_s\frac{dG_s}{dR}\exp(-2\gamma_0R) \tag{8}$$

The total energy available for conversion to Lg is the integral of this equation. To determine the dynamic solution for Rg to Lg scattering, we equate the energy lost from Rg to the energy gained by Lg at each point R. Equation 8 represents the Rg energy loss and the derivative of equation 7 represents the energy gain, so

$$4\omega^2\pi^3\sum_{i=1}^{N}\left|\alpha_i(\omega)^2\right|I_1^i\left|\int_0^R dRJ_0(k_iR)\exp(-ik_0R)S(\omega,R)\right|^2=-\int_0^R\frac{d}{dR}T_0dR \qquad (9)$$

The right hand side of this equation can be calculated for each point given a form for G_s, for example $\exp(-\gamma_s R)$. Equation 9 can be solved for small kR:

$$S(\omega,R)=\frac{1}{2\pi}\frac{\sqrt{\gamma_s(\gamma_s+\gamma_0)}B(\omega)\exp(-2\gamma_sR-2\gamma_0R)}{\sqrt{1-\exp(-2\gamma_sR-2\gamma_0R)}},\ B(\omega)=\left(\left|A_0(\omega)\right|^2 I_1^0\Big/\sum_{i=1}^{N}\left|\alpha_i(\omega)\right|^2 I_1^i\right)^{1/2} \qquad (10)$$

Equation 9 is an integral equation for S, which can be solved numerically, starting with equation 10 for small R, and then used to calculate Lg using (6). Our plan is to calculate Rg-to-Lg scattering using this technique for a range of earth structures and scattering rates.

Shear wave generation by Azgir tamped and decoupled explosions

On December 22, 1971, a 64 Kt tamped nuclear explosion at 987 m depth in salt created a 38 m horizontal radius by 33 m vertical radius cavity in salt at the Soviet Azgir test site. On March 29, 1976, A 10 kt explosion was detonated in the cavity and was recorded at 4 of the same 3-component stations that had recorded the tamped explosion. We examine differences in shear waves between records, which can be attributed to differences between the sources. The most useful set of records are at 17.8 km, where distinct P, S, and Rg phases can be identified.

The tamped and decoupled explosions overlay nearly identically at 0.2 to 0.5 Hz (not shown), where a very slow Rg phase dominates. This provides a constraint on sediment thickness and velocity in our modeling. Up to ~3 Hz, the tamped and decoupled seismograms are very similar (Figure 8). At higher frequencies however, the tamped explosion generates much more shear wave energy. This suggests different mechanisms for shear wave generation at low and high frequencies, shared by both tamped and decoupled explosions at low frequencies only.

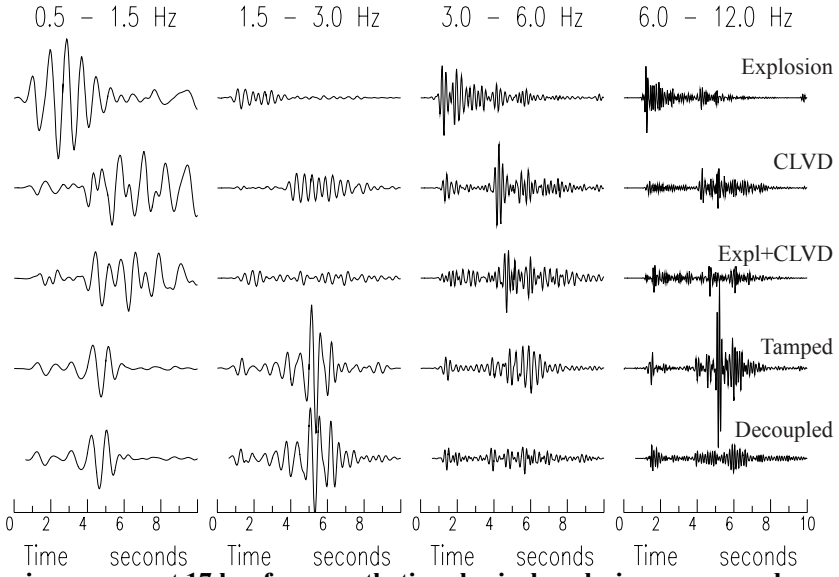

Figure 8. Vertical seismograms at 17 km from synthetic spherical explosion source and compensated linear vector dipole (CLVD) calculations (upper two traces), the sum of those two (middle), and the tamped and decoupled explosions in 4 passbands. Each of the synthetics is scaled by the P-wave rms amplitude of the sum of the explosion and CLVD source, in each passband, and the tamped and decoupled records are scaled by their P-wave rms amplitude.

To determine whether the S-wave observations can be easily modeled with a spherical point explosion in a reasonable velocity structure, and if not, how large an S-wave source the data require, we calculated wavenumber synthetic seismograms for spherical explosion and CLVD sources for a number of models. The models range from a very simple homogeneous salt dome, to a complex, strongly layered model based on the velocity structure for a

7/21/84 explosion at the Lira test site (Murphy et al, 2001), which is north of Azgir. That structure is strongly layered, with highly variable Poisson's ratio. The explosion was in salt at 987 m depth. The sediment thickness was modified to match the observed large, slow Rg. The deeper structure is from the Stevens et al. (2004a) global earth model from surface waves. The fine details of this model are not important, as it would be impossible to uniquely determine the structure from the data, but are simply chosen to allow us to most easily compare the observed P and S phases with the synthetics, by ensuring similar timing, while assessing whether the complex structure can produce the secondary phases observed in the explosion data. We place the CLVD at 650 m depth within a salt layer, rather than in the one of the much higher velocity anhydrite layers. For the range of complex models used here, the observed S-waves were not produced by conversion from a spherical point explosion.

CONCLUSIONS AND RECOMMENDATIONS

Analysis of Degelen nuclear explosion records from BRVK at 650 km indicates that Pn, the entire P wavetrain (Pn through 5.4 km/s, Sn, Lg (3.6 to 3.0 km/s), and Lg coda (3.0 to 2.5 km/s) vary similarly with yield. Their yield dependence can be well fit by the relation slope = 0.855 - 0.034*f, where f is frequency. Amplitudes of Lg coda (3.0 to 2.5 km/s) and the entire P wavetrain (Pn arrival to 5.4 km/s) generally correlate with yield more accurately than do Lg or Sn. There is no apparent dependence of any phase amplitudes on depth, or the extent to which an event is underburied. Non-linear source calculations predict this observation, despite significant differences in the nature of the permanent deformation around cavities of 20% and 50% underburied explosions. We intend to perform similar analysis of Balapan records, for which we have obtained new yield and depth information.

IDG has delivered near source tabular data for 10 historical Degelen nuclear explosions, local seismic records from 4 Balapan and 1 Degelen explosion, and yields and depths the events. We intend to perform more detailed analyses as the dataset increases in size. The near source tabular data will permit exploration of the effect of previous nearby explosions on rock strength and pulse shape. The local measurements, and new depth and yield information, will permit a more detailed assessment of the relationships between the phase amplitudes of local and regional records and source depths, yields, and depth/scale depth ratios for a greater range of values than has previously been possible.

We have derived a solution for the dynamic problem of Rg-to-Lg scattering in which the loss of energy at a point R is directly converted to Lg, and are preparing to perform calculations for different regions, where Rg decay rates will constrain the calculations, and results can be compared with regional Lg observations.

Analysis and modeling of local seismic records indicates that below ~3 Hz, tamped and decoupled explosions generate very similar shear waves in size (relative to P) and shape, whereas the S/P ratio of the decoupled explosion records decreases and that of the tamped explosion increases dramatically at higher frequencies. This suggests that a similar mechanism generates the low frequency shear waves from both tamped and decoupled explosions, while a mechanism not present in the decoupled explosion generates the high frequency shear waves for the tamped explosion.

REFERENCES

Murphy, J. R., I. O. Kitov, B. W. Barker, and D. D. Sultanov (2001), Seismic source characteristics of Soviet peaceful nuclear explosion, *Pure and Applied Geophysics*, 158: 2077–2101.

Stevens, J. L., N. Rimer, H. Xu, G. E. Baker and S. M. Day (2003), Near field and regional modeling of explosions at the Degelen Test Site, SAIC final report to DTRA, SAIC-02/2050, January.

Stevens, J. L., D. A. Adams, G. E. Baker, M. G. Eneva and H. Xu (2004a), Improved surface-wave dispersion models, amplitude measurements, and azimuth estimates, in *Proceedings of the 26th Seismic Research Review: Trends in Nuclear Explosion Monitoring,* LA-UR-04-5801, Vol. 1, pp. 170-180.

Stevens, J. L., G. E. Baker, H. Xu, T. J. Bennett, N. Rimer and S. M. Day (2004b), The Physical Basis of Lg Generation by Explosion Sources, SAIC Final Report submitted to the National Nuclear Security Administration under contract DE-FC03-02SF22676, December.

Takeuchi, H., and M. Saito, (1972), Seismic surface waves, *Methods Comput. Phys*. 11: 217–295.